Investigation of Structural, Spectral, and Dielectric Properties of Cd-Substituted NiCoPr Nano Ferrites

Alina Manzoor[1*], Muhammad Abubakar[1], Amir Muhammad Afzal[2], Muhammad Imran Arshad[1], M. Nasir Rasul[3]

[1] Department of Physics, Government College University, Faisalabad,38000, Pakistan
[2] Department of Physics, Riphah International University, 13-Km Raiwind Road, Lahore-54000 Pakistan
[3] Institute of Physics, The Islamia University of Bahawalpur, Bahawalpur-63100, Pakistan

ARTICLE INFO

ABSTRACT

The effect of cadmium ions on the structural, spectral, and dielectric properties of Pr doped $Ni_{0.4}Co_{0.6-x}Cd_xFe_{1.95}Pr_{0.05}O_4$ ferrites synthesized by the self-ignited sol-gel process is investigated in the present work. The addition of cadmium ions in place of cobalt ions resulted in an increase in the lattice constant. X-ray diffraction experiment revealed the single-phase spinel structure. The obtained average crystallite size is ranging from 20 - 30 nm. By increasing the substitution of cadmium ions, the dielectric constant, dielectric loss (tan δ) and impedance are noted to increase. SEM study found the spherical grain morphology with some degree of agglomeration. The existence of pores, the sintering process, and the magnetic activity of the particles may be responsible for nanosized particles with a homogeneous particle size distribution. Raman spectra revealed a slight shifting in Raman modes with cadmium addition which may be attributed to the strain produced due to the presence of larger cadmium ions at the Fe^{3+} site.

*Corresponding Author's Email: alinamanzoor@gmail.com

1.   Introduction

In the field of nanotechnology, devices and systems are designed, characterized, and implemented by regulating the shape and size of the materials. These controlled-sized materials are immensely used for industrial and domestic applications such as imaging, mechanical industries, telecommunication, catalysis, medical and environmental applications. Thus, nanotechnology advances the fundamental principles of nano-scale materials and their applications (Devan, Kolekar, & Chougule, 2006). With the decrease of particle size, the surface area of nano-sized materials increases which steer the quantum-size effect (Zhang et al., 2020). Due to the growing surface area, that is the principal navigating force to reduce sintering-temperature of the particles, and this reduces the free energy during sintering (Akhtar, Nazir, Tahir, Qamar, & Khan, 2020). The specific chemical and physical properties of nanoparticles make them highly appropriate for the design of new and improved materials and devices.

Spinel ferrites are commonly used to monitor the propagation direction, frequency, amplitude, and phase of microwave signals in microwave devices. To maximize the construction of these devices and to aid in the production of ferrite, a precision measurement of dielectric and magnetic properties at working frequencies and temperature ranges is needed to work out (Lassoued & Li, 2020). In view of applications, the ferrites have become more fascinating because of their high resistivity values (10^2 - 10^{10} ohm-cm) that are nearly 15 times higher in magnitude than iron (Varma, Bharadwaj, & Babu, 2019).

Their applicability at high frequency, good resistance to heat, and greater corrosion resistance are other reasons that make them most significant. Ferrites are excellent soft magnetic materials for high-frequency applications due to low cost, high resistivity, and low eddy current losses that have been thoroughly tested for the application of multi-layer chip inductors (MLCI) (Junaid et al., 2020). The incorporation of rare earth (RE) ions in the lattice of spine ferrites leads to the RE-Fe linkage (4f-3d coupling), the reason behind the changes in the Curie temperature and magnetization of ferrites (Elayakumar et al., 2019). Moreover, the substitution of transition elements into a spinel structure drastically affects the structural, optical, magnetic, and dielectric properties (Pan, Sun, Han, Zhang, & Zhao, 2019).

There are different methods to fabricate the nanocrystalline ferrites like sol-gel auto combustion or controlled combustion method, co-precipitation method, solid state reaction, and hydro-thermal methods etc. (Akhtar, Babar, Qamar, ur Rehman, & Khan, 2019; El Nahrawy, Soliman, Sakr, & El Attar, 2018; Huq, Saha, Ahmed, & Mahmood, 2013; Jalilvand & Faghihi-Sani, 2013). Among these, sol-gel is the most suitable method due using inexpensive precursors, good morphology, easy of handling, controlled size of particles, controlled composition, and homogeneity along with other advantages such as cost-effective method, highly reactive powder, low external energy consumption, and no need of special equipment.

2.   Experimental

Single phase Cd-substituted $Ni_{0.4}Co_{0.6-x}Cd_xFe_{1.95}Pr_{0.05}O_4$ (x=0-0.6) nano-ferrites were synthesized via sol-gel self-ignition technique. The balanced stoichiometric amounts of all salts were taken. Citric acid with 1:1 M ratio was added into the nitrate solution as an oxidizing agent. The solution was stirred for 15-20 minutes to achieve a homogeneous solution and after that small amount of ammonia solution was added to attain pH 7 of the solution. The solution was constantly stirred with heating ON at 250 °C. The solution was converted into thick gel within 1 hour and after some time the auto combustion took place, and fluffy dark grey ferrite ash was collected. After fine grinding of grey ferrite powder, sintering was carried out at 900 °C.

The final fine-grinded sintered samples were characterized through different techniques and their various properties were investigated in detail. XRD experiment was done to analyze the structural properties of material including crystalline size, lattice constant, cell volume, and X-ray density etc. The dielectric properties were analyzed through LCR technique. In order to explore the material's morphology, chemical composition, and crystalline structure, scanning electron spectroscopy (SEM) was used. For the imaging of samples, secondary electrons and back-scattered main electrons are used. Intra- and inter-molecular vibrational information is provided by Raman spectroscopy which also provided the additional understanding of reactions that are useful for material identification.

3.   Results and Discussion
3.1.   XRD Analysis

The X-ray diffraction patterns of all samples of Cd-substituted $Ni_{0.4}Co_{0.6-x}Cd_xFe_{1.95}Pr_{0.05}O_4$ (x=0-0.6) are shown in figure 1. All necessary diffraction peaks can be seen from these XRD patterns that correspond to different planes; specified as (220), (311), (400), and (511). It is determined from these miller indices that the fabricated materials have a face centered cubic structure belonging to space group Fd3m (Valenzuela, 2012). The most intense diffraction peak (311) is found at 35.6 ° which considered as the characteristics peak of the spinel matrix. The recorded patterns are well matched with an ICDD card reference number 00-010-0325.

It is observed that the lattice constant is changed enormously by changing the composition of the samples in figure 2. The value of lattice constant first increases for x=0.15 and after that it decreases for x up to 0.6. This decreasing effect is attributed to the smaller ionic radii of cadmium ions than that of the cobalt ions. The decrease in the lattice constant is primarily due to the contraction of the spinel lattice since the lattice starts to

13

contract when smaller size Cd ions tried to replace the larger sized Co ions (Modak, Ammar, Mazaleyrat, Das, & Chakrabarti, 2009).
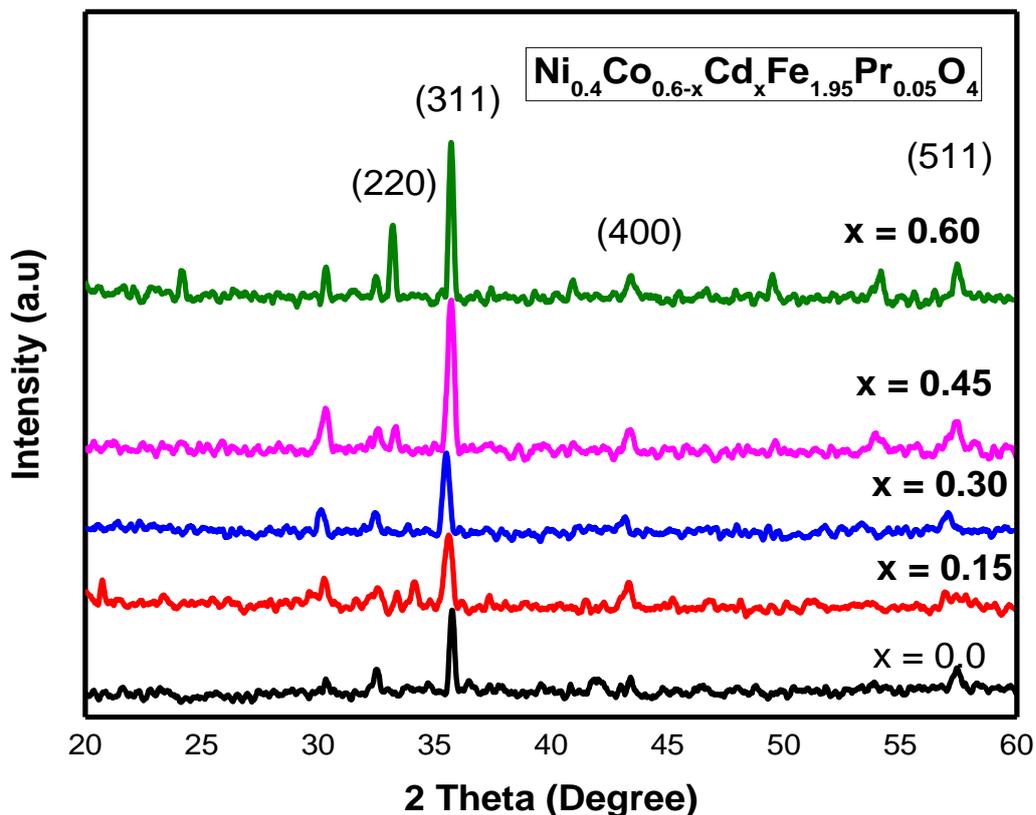

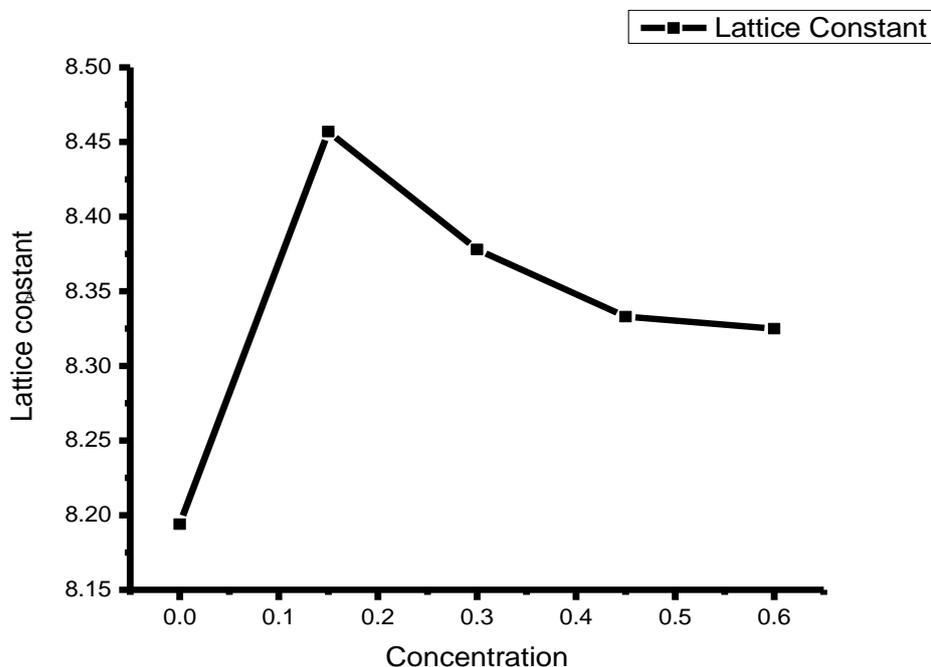**Figure 1: Combine XRD patterns of Ni$_{0.4}$Co$_{0.6-x}$Cd$_x$Fe$_{1.95}$Pr$_{0.05}$O$_4$ ferrites**

Figure 2: Graph between concentration and lattice constant

The crystallite size (*D*) from each peak is calculated and then an average value of *D* is taken for each sample. The average value of crystallite size is ranging from 20-30 nm. A nonlinear variation in *D* is observed as a function of Cd concentration. Figure 3 represents the variation of crystallite size as a function of Cd concentration. It is observed that from the concentration x = 0 to x = 0.15 the crystallite size is drastically reduced and after that it increases.
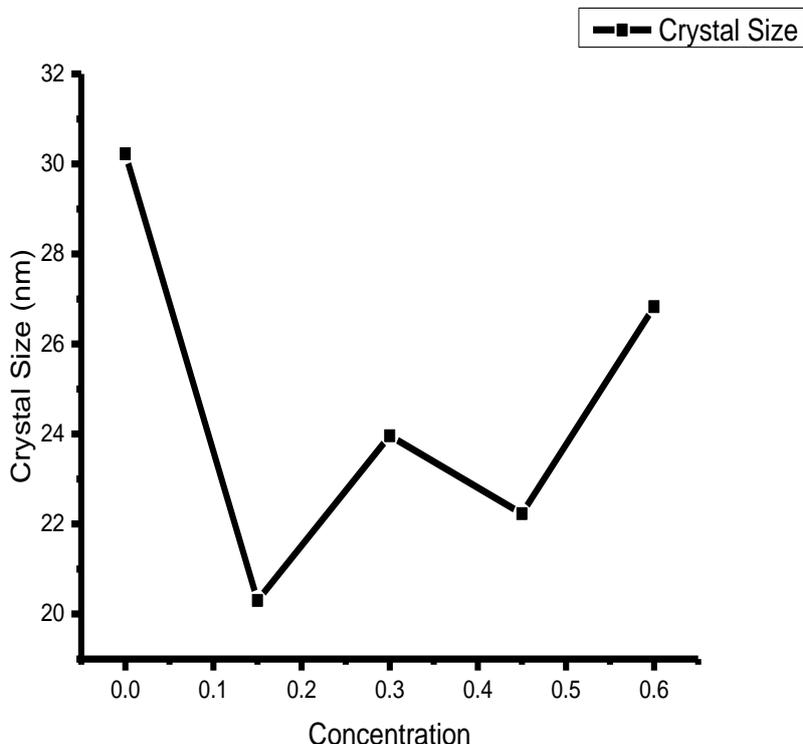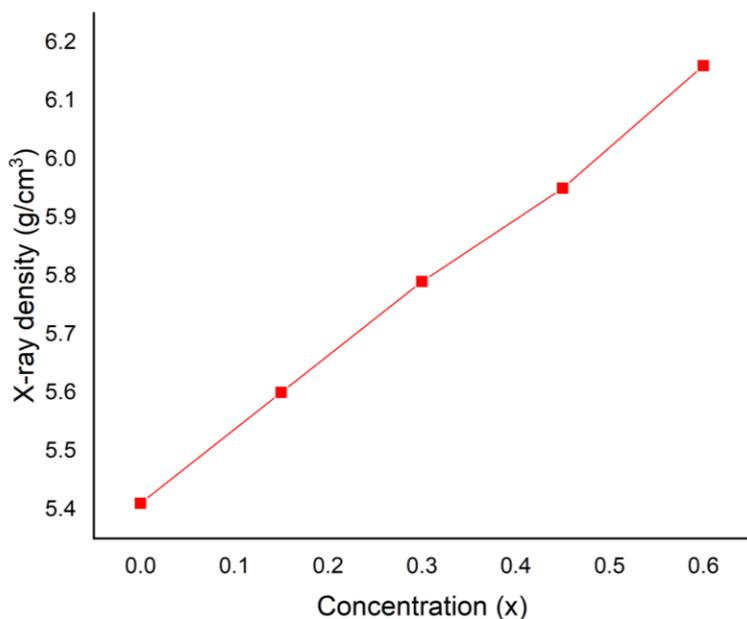
Figure 3: Graph between concentration and average crystallite size

The X-ray density is calculated using the following relation.

$$\rho_x = 8M/Na^3 \tag{1}$$

Here, *M* is the molecular weight of the composition, *N* is the Avogadro number, and *a* is the lattice constant.

The value of X-ray density is ranging from 5.41 to 6.16 g/cm^3. It is observed that with increasing Cd substitution, the X-ray density is also increased. This increase in the X-ray density is due to the fact that the X-ray density is directly dependent on the molecular weight as well as on the lattice parameter (Gupta & Coble, 1968). As we have noticed that the lattice constant is decreased with the concentration while the atomic mass of Cd (112.4 amu) is greater than that of Co (58.93 amu). So, it is expected to increase the X-ray density.

Figure 4: Graph between concentration and X-ray density

3.2. SEM Study

Scanning electron micrographic (SEM) images of representative ferrites samples doped with Cd and rear earth praseodymium showed the surface morphology (figures 5a-5e). Samples are sintered at 900 °C and clusters of fine agglomerated spherical particles of uneven size are found almost homogeneously and uniformly distributed. The agglomeration is observed to reduce by increasing the Cd substitution. The replacement of Co by Cd leads to enhance the crystallinity of the materials. The agglomeration indicates the porous nature, particles of nanometer sizes, and a homogenous particle size distribution that can be responsible for the magnetic behavior of the particles. Analysis of the SEM images for cobalt ferrites doped with Cd and Pr showed that the samples are composed of smaller grains. These results are in line with the calculated Scherrer crystallite dimension, as discussed above, using the XRD data for cadmium doped cobalt ferrites.
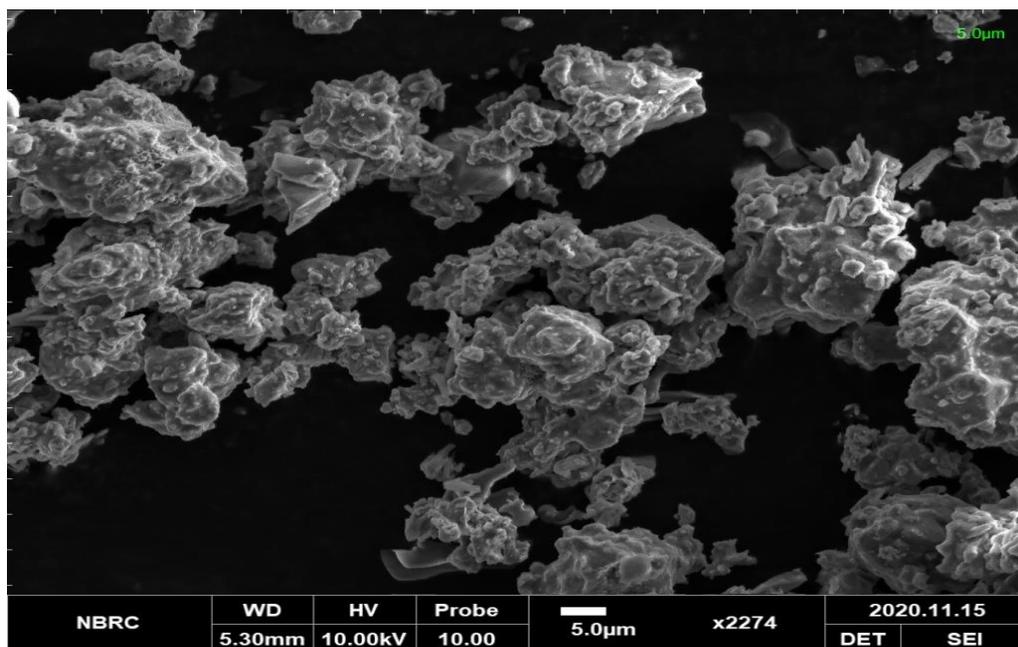

Figure 5a: SEM image of $Ni_{0.4}Co_{0.6}Fe_{1.95}Pr_{0.05}O_4$ ferrite

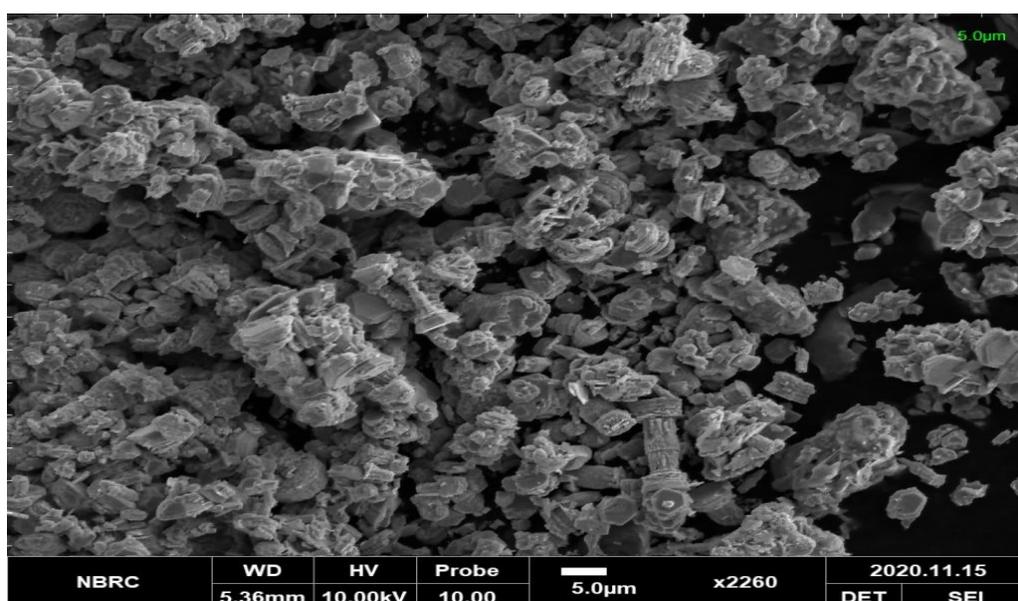**Figure 5b: SEM image of $Ni_{0.4}Co_{0.45}Cd_{0.15}Fe_{1.95}Pr_{0.05}O_4$ ferrite**
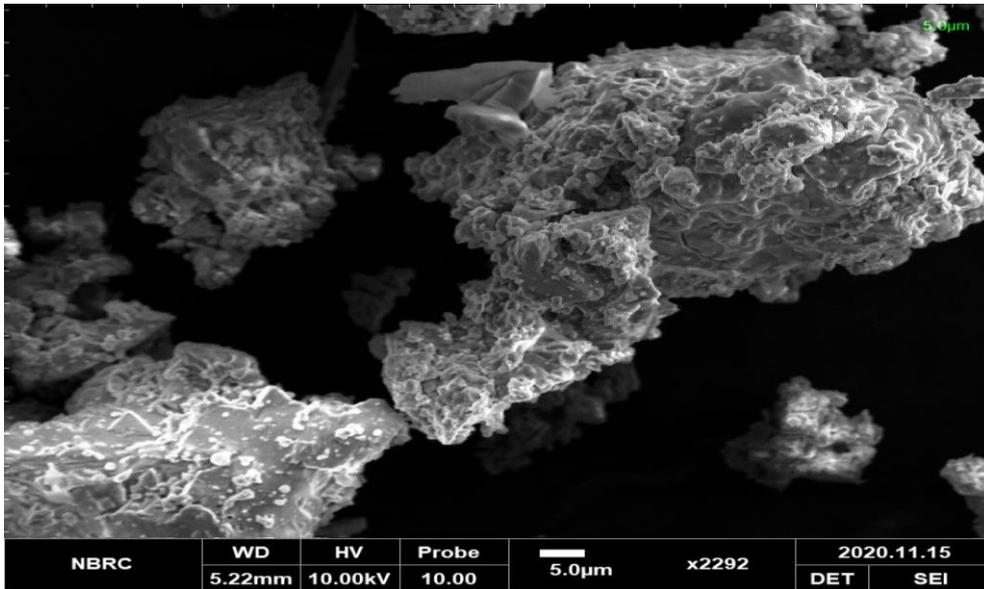
Figure 5c: SEM image of Ni$_{0.4}$Co$_{0.30}$Cd$_{0.30}$Fe$_{1.95}$Pr$_{0.05}$O$_4$ ferrite
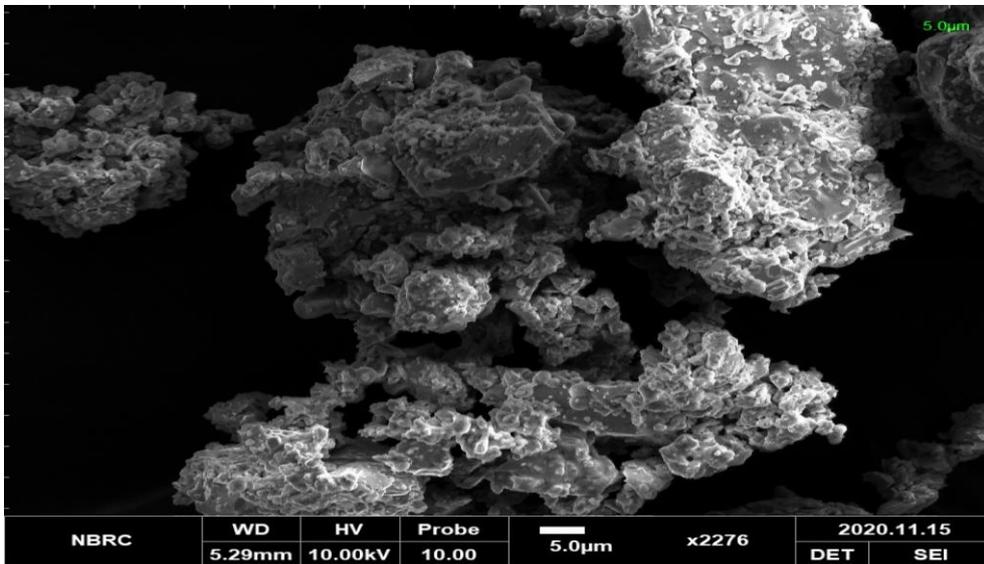
Figure 5d: SEM image of Ni$_{0.4}$Co$_{0.15}$Cd$_{0.45}$Fe$_{1.95}$Pr$_{0.05}$O$_4$ ferrite
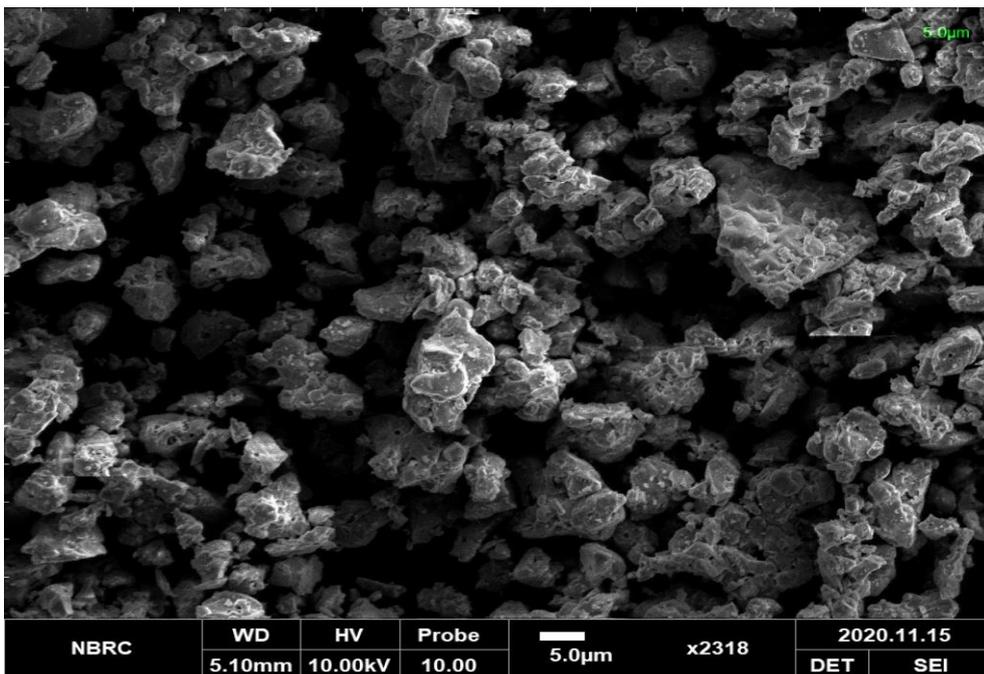
Figure 5e: SEM image of Ni$_{0.4}$Cd$_{0.60}$Fe$_{1.95}$Pr$_{0.05}$O$_4$ ferrite

3.3. Raman Spectroscopy

The Raman spectra of $NiCoFe_2PrO_4$ nano particles substituted by Cd^{2+} are shown in the figure 6. The Cd^{2+} ions have greater ionic radius to occupy the tetrahedral (A) site due to which the structural disorder of the sublattice of oxygen has increased. All 6 Raman active modes assigned as $2A_{1g}$ ($596 - 613$ cm^{-1}, $672 - 688$ cm^{-1}), E_g ($292 - 305$ cm^{-1}), $3T_{2g}$ ($538 - 574$ cm^{-1}, $454 - 467$ cm^{-1}, $200 - 250$ cm^{-1}) can be seen in the spectra. A 1g active mode, usually referred to as the shoulder A_{1g} (2), is a function of spinal ferrite reverse and combined. The vibration models of over 600 cm^{-1} conduct to stretch symmetrically the metal oxygen bond of the tetrahedral sites and to bend oxygen at octahedral positions in modes under 600 cm^{-1}; both symmetrically and unsymmetrically. A slight shifting activity is found in Raman modes with cadmium substitution that can be attributed to the strain caused by the inclusion of the broader cadmium ions at the Fe^{3+} site. The tetrahedral site is symmetrically bent with Fe ion in relation to an oxygen atom by the Fe-O mode (Haque, Huq, & Hakim, 2008; Rahman & Ahmed, 2005).
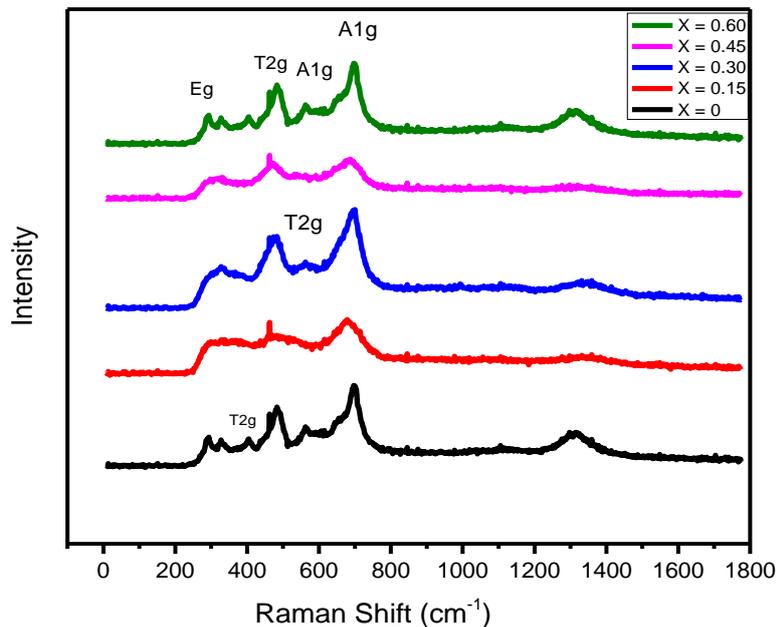
Figure 6: Raman scattering of $Ni_{0.4}Co_{0.6-x}Cd_xFe_{1.95}Pr_{0.05}O_4$ ferrites

3.4. Dielectric Study

The room-temperature dielectric measurements are taken for a frequency range of 1 KHz to 10^7 Hz. The figure 7 has shown the variation in dielectric constant ($\acute{\epsilon}$) as a function of frequency (f) of the AC field applied. It shows the conductive behavior of un-doped and Cd doped cobalt ferrites. At lower frequencies, the value of dielectric constant is observed to be high which further decreases with increasing the frequency of applied field. This is a typical behavior of ferrites, already investigated and reported by various researchers (Akhtar et al., 2020; Caltun, Spinu, & Stancu, 2001). The contribution to conduction phenomenon in ferrites comes from four major processes; polarization contributions at lower frequencies, i.e., dipolar and space charge, electrical, ionic, and some of the polarization contributions at higher frequencies, allowing the dielectric constant ($\acute{\epsilon}$) to decrease. The space-charge polarization model holds two parts: the grains (more conductive layer) and grain boundaries (less conductive and more resistive). The accumulation of space charge carriers in a dielectric medium is preferred to move through a resistive part (grain boundaries) of the sample. So, a finite time is required by the charge carriers to position their axes in the direction of alternating electric field. Thus, by increasing the frequency, the charge carrier remained incapable to sustain with the field reversals and consequently dielectric constant starts to decrease (Nam, Jung, Shin, & Oh, 1995; Pardavi-Horvath, 2000).
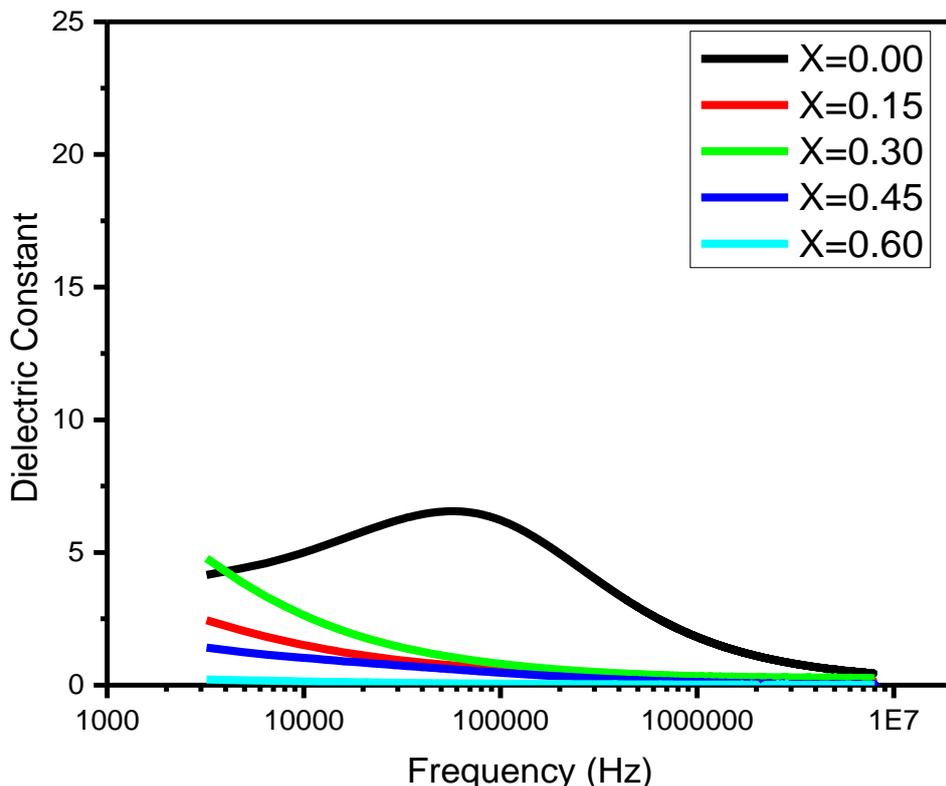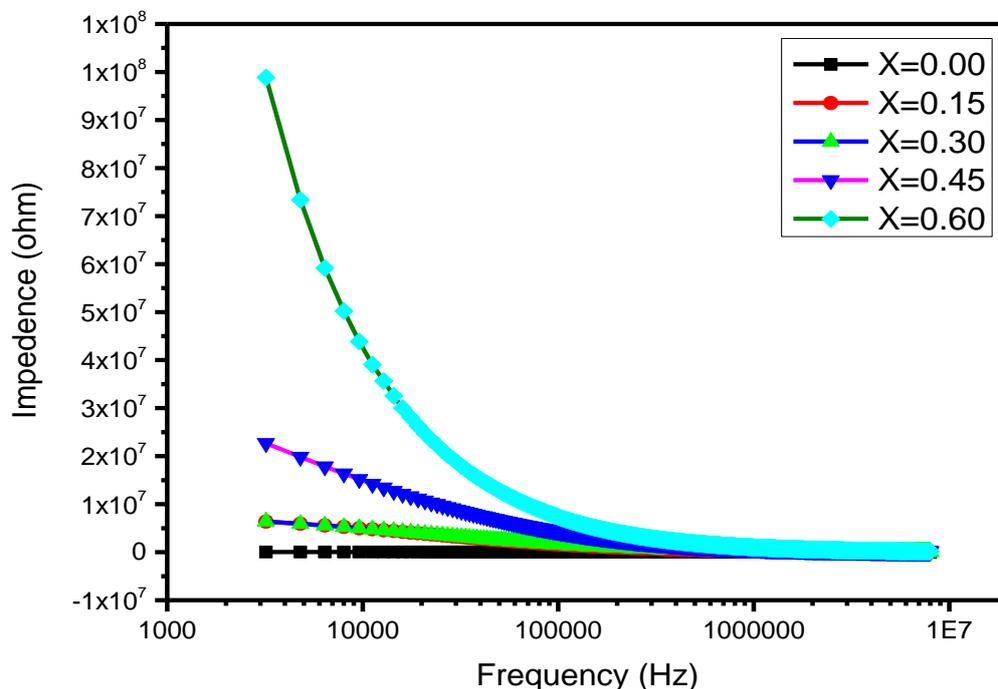
Figure 7: Graph between frequency and dielectric constant

The overall value of dielectric constant is observed to decrease with an increase in Cd concentration. In addition, in nanosized ferrites, the number of grain boundaries are larger which causes high dielectric constant at lower frequencies, whereas low-dielectric grains at high frequencies have more contribution (Byun, Byeon, Hong, & Kim, 1999). The variation of loss tangent loss as a function of applied field frequency for all samples is represented in figure 8. It can be seen that the loss tangent is increases as the concentration of Cd ions increases while it increases with increasing the applied field frequency.
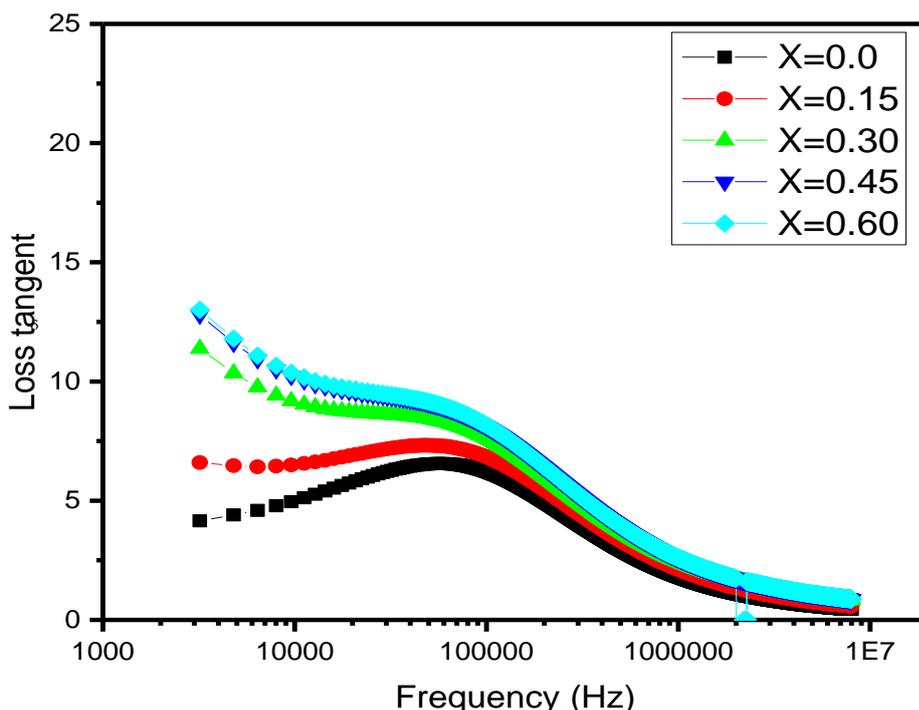
Figure 8: Graph between frequency and loss tangent

The variation in impedance as a function of applied field frequency for all samples is represented in figure 9. The value of the impedance decreases as the applied field frequency increases, and it becomes almost constant at a point and seems to be independent of the frequency. By increasing the concentration of Cd ions, the value of impedance is also increased. For x > 0.45, there is a sudden increase in the impedance value.

Figure 9: Graph between frequency and impedance

4.   Conclusion

Cd-substituted $Ni_{0.4}Co_{0.6-x}Cd_xFe_{1.95}Pr_{0.05}O_4$ (x=0-0.6) nano-ferrites synthesized via sol-gel method are investigated for various properties. XRD results confirmed the development of fcc spinel structure with crystallite sizes ranging from 20 to 30 nm. The incorporation of Cd at Co positions leads to an increase in lattice constant from 8.194 Å to 8.457 Å and a decrease in X-ray density. Dielectric constant observed to decrease while impedance of materials noted to increase with increase in Cd substitution. SEM analysis confirmed the spherical morphology of the constituted grains with some degree of agglomeration. A slight shifting in Raman modes has observed due to the presence of greater ionic radius of Cd at the Fe^{3+} sites. Due to the Fe-O mode, the perfectly straight bending of the oxygen ions with respect to the Fe ions at the tetrahedral site is detected.

References

Akhtar, M. N., Babar, M., Qamar, S., ur Rehman, Z., & Khan, M. A. (2019). Structural Rietveld refinement and magnetic features of prosademium (Pr) doped Cu nanocrystalline spinel ferrites. *Ceramics International, 45*(8), 10187-10195. doi:10.1016/j.ceramint.2019.02.069

Akhtar, M. N., Nazir, M. S., Tahir, Z., Qamar, S., & Khan, M. A. (2020). Impact of Co doping on physical, structural, microstructural and magnetic features of MgZn nanoferrites for high frequency applications. *Ceramics International, 46*(2), 1750-1759. doi:10.1016/j.ceramint.2019.09.149

Byun, T. Y., Byeon, S. C., Hong, K. S., & Kim, C. K. (1999). Factors affecting initial permeability of Co-substituted Ni-Zn-Cu ferrites. *Ieee transactions on magnetics, 35*(5), 3445-3447. doi:10.1109/20.800552

Caltun, O. F., Spinu, L., & Stancu, A. (2001). Magnetic properties of high frequency Ni-Zn ferrites doped with CuO. *Ieee transactions on magnetics, 37*(4), 2353-2355. doi:10.1109/20.951170

Devan, R., Kolekar, Y., & Chougule, B. (2006). Effect of cobalt substitution on the properties of nickel–copper ferrite. *Journal of Physics: Condensed Matter, 18*(43), 9809.

El Nahrawy, A., Soliman, A., Sakr, E., & El Attar, H. (2018). SODIUM-COBALT FERRITE NANOSTRUCTURE STUDY: SOL-GEL SYNTHESIS, CHARACTERIZATION, AND MAGNETIC PROPERTIES. *Journal of Ovonic Research, 14*(3).

Elayakumar, K., Manikandan, A., Dinesh, A., Thanrasu, K., Raja, K. K., Kumar, R. T., . . . Baykal, A. (2019). Enhanced magnetic property and antibacterial biomedical activity of Ce3+ doped CuFe2O4 spinel nanoparticles synthesized by sol-gel method. *Journal of Magnetism and Magnetic Materials, 478*, 140-147. doi:10.1016/j.jmmm.2019.01.108

Gupta, T., & Coble, R. (1968). Sintering of ZnO: I, Densification and grain growth. *Journal of the American Ceramic Society, 51*(9), 521-525. doi:10.1111/j.1151-2916.1968.tb15679.x

Haque, M. M., Huq, M., & Hakim, M. (2008). Influence of CuO and sintering temperature on the microstructure and magnetic properties of Mg–Cu–Zn ferrites. *Journal of Magnetism and Magnetic Materials, 320*(21), 2792-2799. doi:10.1016/j.jmmm.2008.06.017

Huq, M., Saha, D., Ahmed, R., & Mahmood, Z. (2013). Ni-Cu-Zn ferrite research: A brief review. *Journal of Scientific Research, 5*(2), 215-234. doi:10.3329/jsr.v5i2.12434

Jalilvand, G., & Faghihi-Sani, M.-A. (2013). Fe doped Ni–Co spinel protective coating on ferritic stainless steel for SOFC interconnect application. *International Journal of Hydrogen Energy, 38*(27), 12007-12014. doi:10.1016/j.ijhydene.2013.06.105

Junaid, M., Khan, M. A., Abubshait, S. A., Akhtar, M. N., Kattan, N. A., Laref, A., & Javed, H. M. A. (2020). Structural, spectral, dielectric and magnetic properties of indium substituted copper spinel ferrites synthesized via sol gel technique. *Ceramics International, 46*(17), 27410-27418. doi:10.1016/j.ceramint.2020.07.227

Lassoued, A., & Li, J. (2020). Magnetic and photocatalytic properties of Ni–Co ferrites. *Solid State Sciences, 104*, 106199. doi:10.1016/j.solidstatesciences.2020.106199

Modak, S., Ammar, M., Mazaleyrat, F., Das, S., & Chakrabarti, P. (2009). XRD, HRTEM and magnetic properties of mixed spinel nanocrystalline Ni–Zn–Cu-ferrite. *Journal of Alloys and Compounds, 473*(1-2), 15-19. doi:10.1016/j.jallcom.2008.06.020

Nam, J., Jung, H., Shin, J., & Oh, J. (1995). The effect of Cu substitution on the electrical and magnetic properties of NiZn ferrites. *Ieee transactions on magnetics, 31*(6), 3985-3987. doi:10.1109/20.489838

Pan, X., Sun, A., Han, Y., Zhang, W., & Zhao, X. (2019). Structural and magnetic properties of Bi 3+ ion doped Ni–Cu–Co nano ferrites prepared by sol–gel auto combustion method. *Journal of Materials Science: Materials in Electronics, 30*(5), 4644-4657. doi:10.1007/s10854-019-00757-8

Pardavi-Horvath, M. (2000). Microwave applications of soft ferrites. *Journal of Magnetism and Magnetic Materials, 215*, 171-183. doi:10.1016/S0304-8853(00)00106-2

Rahman, I., & Ahmed, T. (2005). A study on Cu substituted chemically processed Ni–Zn–Cu ferrites. *Journal of Magnetism and Magnetic Materials, 290*, 1576-1579. doi:10.1016/j.jmmm.2004.11.250

Valenzuela, R. (2012). Novel applications of ferrites. *Physics Research International, 2012*.

Varma, M. C., Bharadwaj, S., & Babu, K. V. (2019). Observation of anomalous site occupancy in Ni-Co-Cu-Cr ferrite system synthesized by sol-gel method. *Physica B: Condensed Matter, 556*, 175-182. doi:10.1016/j.physb.2018.12.002

Zhang, W., Sun, A., Zhao, X., Pan, X., Han, Y., Suo, N., . . . Zuo, Z. (2020). Structural and magnetic properties of Ni–Cu–Co ferrites prepared from sol-gel auto combustion method with different complexing agents. *Journal of Alloys and Compounds, 816*, 152501. doi:10.1016/j.jallcom.2019.152501